

Fig. S-1. High resolution transmission electron microscopy (HRTEM) of chitosan-coated $Mg_{1-x}Co_xFe_2O_4$ ($0 \leq x \leq 1$ with $\Delta x = 0.1$) nanoparticles in the as-synthesized condition. HRTEM images indicate that the nanoparticles are crystalline for all values of x. However, the degree of crystallinity increases with an increase in cobalt content x. Lattice fringes are seen more clearly for higher cobalt content which is because of the higher degree of crystallinity with the increase of Co. The figure also indicates that particle size increases with the increase of cobalt in the $Mg_{1-x}Co_xFe_2O_4$ ($0 \leq x \leq 1$ with $\Delta x = 0.1$) in the as-synthesized condition.

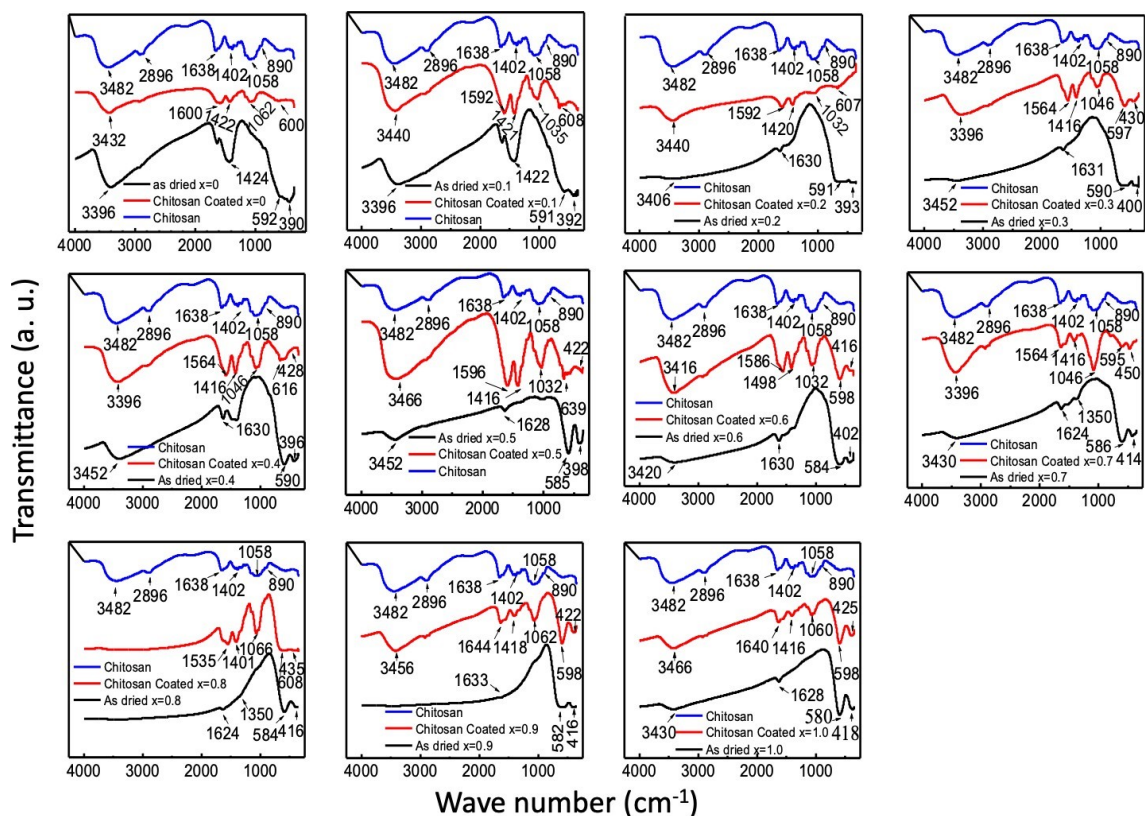


Fig. S-2. FTIR spectrum of chitosan, bare, and chitosan-coated $Mg_{1-x}Co_xFe_2O_4$ nanoparticles in the range of $350-3000\text{ cm}^{-1}$. A small amount of powder samples were mixed with potassium bromide powder and pelletized. The pellets were then placed on the sample holder of attenuated total reflection (ATR) to directly acquire the sample's FTIR spectrum. For bare samples, the frequency of the higher frequency band increases, and that of the lower frequency band decreases with an increase in cobalt content x , which indicates that the bond length of A sites decreases and that of B sites increases with increasing cobalt content. In the case of chitosan-coated particles, both the higher and lower frequency band shifted towards the higher frequency region, which indicates good coating.

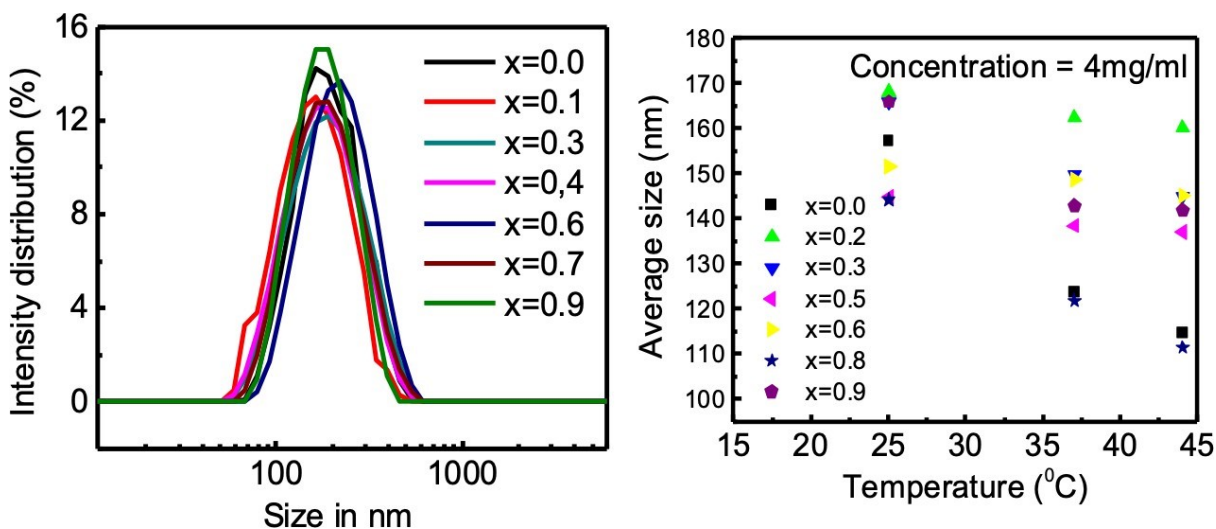


Fig. S-3. (a) Hydrodynamic size distribution of chitosan-coated $Mg_{1-x}Co_xFe_2O_4$ nanoparticles at 25°C . Average hydrodynamic size is independent of cobalt content x . The lower value of the dispersive index confirms that the particles are dispersed and well coated. (b) Variation of average hydrodynamic size with the temperature at the concentration of 4 mg/ml of chitosan-coated $Mg_{1-x}Co_xFe_2O_4$ nanoparticles. At this concentration, the average hydrodynamic size decreases with increasing temperature.

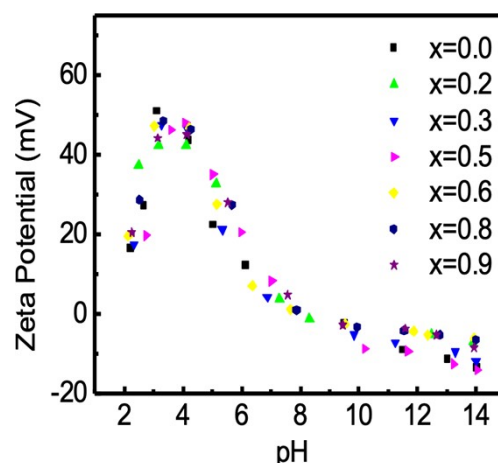


Fig. S-4. The variation of zeta potential of chitosan-coated $\text{Mg}_{1-x}\text{Co}_x\text{Fe}_2\text{O}_4$ nanoparticles with the pH of the solution. The colloidal suspension would be stable in the region of pH 3-5. The colloidal suspension would be the most unstable near pH 8 and above and particles would agglomerate in this region. In the higher pH region, the coating is also unstable.

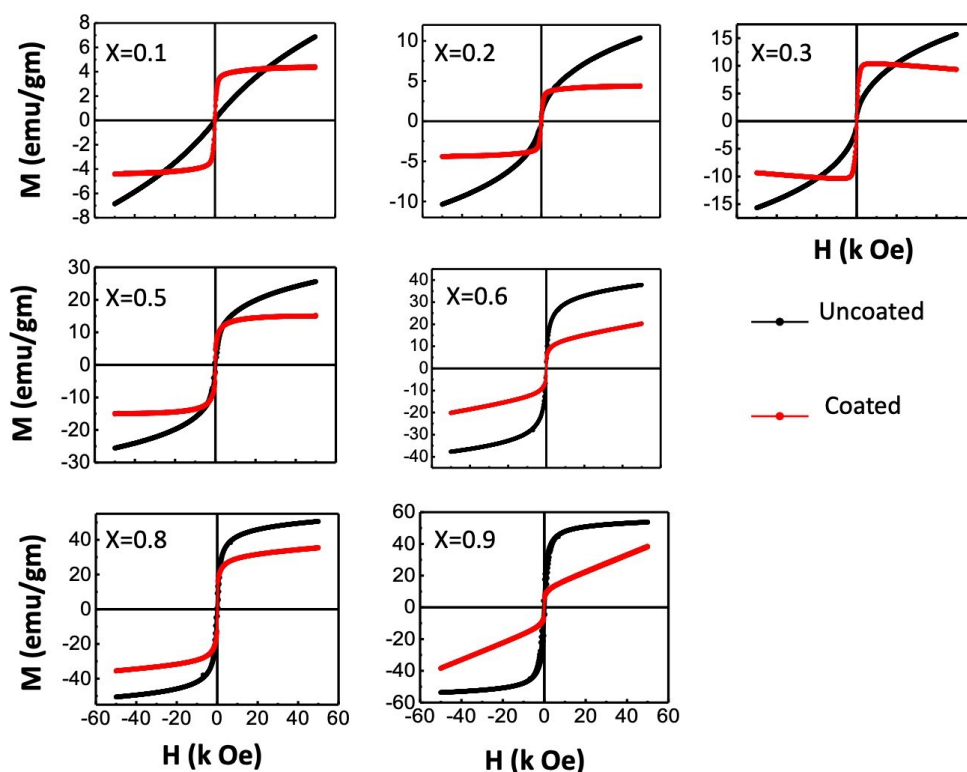


Fig. S-5. M-H loops for bare and chitosan-coated $\text{Mg}_{1-x}\text{Co}_x\text{Fe}_2\text{O}_4$ ($0 \leq x \leq 1$ with $\Delta x = 0.1$) nanoparticles with a maximum magnetic field of 5T. It is interesting to note that the shape of the M-H curves change with composition. The shape also varies between uncoated and coated samples. Extensive variations in the M-H curves of bare and coated samples demonstrate that the nanoparticles of all compositions have undergone surface functionalizations. For lower cobalt content, both bare and coated particles are superparamagnetic. With the increase of x , there is a transition from superparamagnetic to a mixed slow (ferrimagnetic) and fast (superparamagnetic) relaxation in the as-dried condition. Wide variations in the shape of the hysteresis loop between bare and coated nanoparticles might be due to the clustering effect in the coated particles. The surface atoms of nanoparticles affect the magnetic properties of nanoparticles due to the large surface-to-volume ratio. There are incomplete coordination atoms at the surface, and A-B coupling through superexchange interaction mediated by oxygen is broken, for which the surface anisotropy is induced because of the distribution of exchange field and perturbations of crystal field.